Steps, kinetic anisotropy, and long-wavelength instabilities in directional solidification

H. P. Grimm and S. H. Davis
Department of Engineering Sciences and Applied Mathematics, Northwestern University, Evanston, Illinois 60208

G. B. McFadden
National Institute of Standards and Technology, Gaithersburg, Maryland 20899
(Received 30 September 1998)

We consider the effect of anisotropic interface kinetics on long-wavelength instabilities during the directional solidification of a binary alloy having a vicinal interface. Linear theory predicts that a planar solidification front is stabilized under the effect of anisotropy as long as the segregation coefficient is small enough, whereas a novel instability appears at high rates of solidification. Furthermore, the neutral stability curve, indicating the values of the principal control parameter (here the morphological number) for which the growth rate of a sinusoidal perturbation of a given wavelength changes its sign, is shown to have up to three branches, two of them combining to form an isola for certain values of the control parameters. We identify conditions for which linear stability theory predicts the instability of the planar interface to long-wavelength traveling waves. A number of distinguished limits provide evolution equations that describe the resulting dynamical behavior of the crystal-melt interface and generalize previous work by Sivashinsky, Brattkus, and Davis and Riley and Davis. Bifurcation analysis and numerical computations for the derived evolution equations show that the anisotropy is able to promote the tendency to supercritical bifurcation, and also leads to the development of strongly preferred interface orientations for finite-amplitude deformations. [S1063-651X(99)02605-7]

PACS number(s): 64.70.Dv, 81.30.Fb, 47.20.Ky

I. INTRODUCTION

During crystal growth from a fluid phase with a vicinal interface, the interface velocity is generally well-approximated as a linear function of the local undercooling at the interface. For a vicinal surface, the constant of proportionality (the interface-attachment coefficient) is a strongly anisotropic function of the interface orientation. The characteristic effects of interface attachment kinetics contrast with the assumption of local thermodynamic equilibrium; they are manifested in a number of materials processing applications, including vapor growth [1], solution growth [2], and melt growth [3].

For a vicinal surface, the microscopic picture of a crystal-fluid interface consists of a series of atomically flat terraces that are interrupted by steps of roughly atomic dimensions. If the steps are well separated from each other, the mean orientation of the interface then differs only slightly from the singular orientation of the terraces, and the motion of the interface in its normal direction proceeds by layer growth that occurs at the step locations. Therefore, the limiting factors for the growth are the attachment rate at the steps and the step density. This view implies that an interface without steps, which consists entirely of the singular orientation, is stationary, resulting in the strong orientation dependence (anisotropy) of the interface-attachment coefficient for vicinal interfaces. In practice, for large enough undercooling, steps on a singular interface can arise via two-dimensional nucleation of a new layer in the interior of a terrace, and via defects in the surface, such as screw dislocations that act as step sources. Once steps are present on a singular surface, the mean orientation differs from the singular orientation, and motion of the interface in its normal direction can occur at a finite rate as material is added at the steps. In this paper, we investigate the implications of an anisotropic kinetic law given by an attachment coefficient that is directly proportional to the local slope of the interface, measured relative to the singular orientation.

The effect of attachment kinetics on the morphological stability of a growing crystal has received considerable attention (see, e.g., Ref. [4]). For the growth of a pure material into a hypercooled melt, finite attachment kinetics can lead to constant velocity growth; a number of linear and nonlinear analyses of the hypercooled growth with kinetics have been performed [5–7], although the number of experimental studies in this regime is limited [8]. For directional solidification of a binary alloy into a positive temperature gradient, the effect of an isotropic kinetic coefficient is merely to modify the interface temperature; an exchange of linearized stabilities generally holds, and the conditions at the onset of instability are unaffected by kinetic coefficient. The effect of a mild anisotropy is to generate traveling wave instabilities at the onset [9]. The conditions at the onset are again unchanged if the anisotropy is mild enough in which case a quasistatic treatment of the diffusion field is a good approximation, and a weakly nonlinear treatment of the problem [10] predicts the formation of tilted cells in two dimensions. If the kinetic anisotropy is strong enough, however, a quasistatic analysis becomes inadequate, and the onset of instability can be significantly modified. In this case, the effect of the traveling-wave instability is to produce a phase difference between the perturbed interface and the solute field in which lateral solute transport can significantly stabilize the interface [2]. This kinetic stabilization has also been studied in conjunction with shear flows parallel to the interface, which tend to interact strongly with the lateral step motion [3].

In various problems of crystal growth cited above, pat-

terns of long wavelength tend to be favored, suggesting that the morphological stability theory may be extended to include nonlinear effects by taking advantage of the disparate length scales in the directions tangential and normal to the growth direction. Long-wave theories of this general type have been developed for directional solidification studies without kinetics by a number of authors [4]; examples include the work of Sivashinsky [11], Riley and Davis [12], and Brattkus and Davis [13]. A long-wavelength theory that generalizes the work of Sivashinsky by incorporating the effects of weak kinetic anisotropy has been considered by Young, Davis, and Brattkus; Novick-Cohen [14] generalized the treatment of Sivashinsky to include the effects of nonequilibrium thermodynamics and derived a form of the Kuramoto-Sivashinsky equation for long wave instabilities. Hoyle, McFadden, and Davis [15] investigated the effects of surface-tension anisotropy on pattern selection during the solidification of a binary alloy, and Golovin and Davis [16] considered the effect of anisotropic surface tension on the hypercooled growth of a pure material.

In the following section we formulate the governing equations of the model, in particular the anisotropic kinetic law, and discuss the linear theory that describes the morphological stability of the planar state. In Sec. III we consider long-wavelength limits of the governing equations in a variety of limits: First, when including only small effects of anisotropy, we recover the results of Young *et al.*, and then show how a similar scaling may be used to take into account larger effects. We explain why there is no simple extension of the work of Brattkus and Davis and develop a long-wave equation for a somewhat similar scaling which we show to be valid far beyond the limits of the isotropic case. Finally, we use the scalings of Riley and Davis to investigate kinetic anisotropy. Conclusions are presented in Sec. IV.

II. GOVERNING EQUATIONS AND LINEAR THEORY

We consider the one-sided directional solidification of a binary alloy in a reference frame moving with the velocity V of the crystal-melt interface. In this coordinate system, the steady-state planar solution is described by an exponential solute profile

$$C^*(z)=C_\infty\left\{1+\frac{(1-k)}{k}\exp(-Vz/D)\right\}, \tag{1}$$

in the liquid region $0<z<\infty$, where the interface is located at the point $z=0$. Here C_∞ is the bulk concentration in the liquid far from the interface, the distribution coefficient k gives the ratio of the interface concentration in the solid to that in the liquid, and D is the solute diffusivity in the liquid. Diffusion in the solid phase will be neglected, and for simplicity we shall assume that the temperature field is given by a linear function $T(z)$ with a constant temperature gradient $dT/dz=G$.

We shall study a kinetic model that is based on step motion for a vicinal interface, and consider a two-dimensional problem for a nonplanar interface $z=H(x,t)$ and solute field $C^*(x,z,t)$ that satisfy

$$C^*_t-VC^*_z=D(C^*_{xx}+C^*_{zz}), \tag{2}$$

in the liquid region $H(x,t)<z<\infty$. The effects of lateral confinement of the system will be neglected, and solutions that are periodic in x will be assumed. We also impose the far-field boundary condition $C^*\to C_\infty$ as $z\to\infty$. At the crystal-melt interface $z=H(x,t)$ we have conservation of solute

$$-D(C^*_z-H_xC^*_x)=[V+H_t](1-k)C, \tag{3}$$

and the modified Gibbs-Thomson equation

$$\frac{(V+H_t)}{\sqrt{1+H_x^2}}=\beta(H_x)\{T_M+mC^*-T_M\Gamma\mathcal{K}-T(H)\}. \tag{4}$$

Here T_M is the melting point of the pure material, m is the liquidus slope, Γ is the capillary constant, $\mathcal{K}$ is the interface curvature, and β is the anisotropic interface-attachment coefficient. We shall assume that this kinetic coefficient has the form [2]

$$\beta(H_x)=\beta_{st}(\bar{p}+H_x), \tag{5}$$

where $\bar{p}$ represents the orientation of the planar interface $z=0$ with respect to the singular orientation and β_{st} is a constant. The velocity and temperature of the planar interface are therefore related by

$$V=\beta_{st}\bar{p}\left\{T_M+m\frac{C_\infty}{k}-T(0)\right\}. \tag{6}$$

A. The rescaled equations

In order to get dimensionless variables, we rescale lengths with D/V, time with D/V^2, and replace the physical concentration $C^*(x,z,t)$ by $(D\,G_C/V)C(x,z-H(x,t),t)+C_\infty/k$, where $G_C=(V/D)C_\infty(k-1)/k$ is the concentration gradient at the planar interface. Note that we mapped the interface to the plane by replacing the original z coordinate by $z+H$. Furthermore, we introduce the dimensionless parameters

$$\bar{\beta}=\frac{\beta_{st}mG_CD}{V^2},\quad \tilde{\alpha}=\frac{1}{p^2\bar{\beta}},$$

$$\bar{\Gamma}=\frac{T_M\Gamma V^2}{mG_CD^2},\quad M=mG_C/G. \tag{7}$$

Here M is the morphological number, $\bar{\Gamma}$ represents surface energy, and $\bar{\beta}$ represents the magnitude of the attachment kinetics. The diffusion equation for $z>0$ then becomes

$$C_t=C_{xx}+(1+H_x^2)C_{zz}-2H_xC_{xz}+(1+H_t-H_{xx})C_z, \tag{8}$$

the solute balance at the (mapped) interface $z=0$

$$(1+H_x^2)C_z-H_xC_x=(1+H_t)[1-(1-k)C], \tag{9}$$

and the kinetic law at $z=0$

$$\frac{1+H_t}{(1+H_x^2)^{1/2}}=\beta(p+H_x)\left(C+\frac{\Gamma H_{xx}}{(1+H_x^2)^{3/2}}-M^{-1}H\right)+\left(1+\frac{H_x}{p}\right), \tag{10}$$

where for convenience we have dropped the bars. The far-field condition for C is

$$\lim_{z\to\infty} C=1. \tag{11}$$

B. Dispersion relation

These equations admit a basic state $(\overline{C},\overline{H})$ of the form

$$\overline{C}=1-e^{-z}, \quad \overline{H}=0. \tag{12}$$

When investigating the linear stability of the basic state, we introduce perturbations $C'=C-\overline{C}$ and $H'=H-\overline{H}$ into the above equations. The linearized problem in (C',H') may be solved by separating variables to get nontrivial solutions

$$C'=(\gamma e^{-rz}+\eta e^{-z})e^{iax}e^{\sigma t}, \quad H'=\eta e^{iax}e^{\sigma t} \tag{13}$$

under the condition that the following *dispersion relation* holds:

$$M^{-1}=1+\frac{k+\sigma}{1-k-r}-\Gamma a^2+\tilde{\alpha}(ia-p\sigma). \tag{14}$$

Here γ and η are constants, a is the wave number of the perturbation, $\sigma=\sigma_r+i\omega$ is the complex growth rate, and the exponent r is given by

$$r=\frac{1}{2}(1+\sqrt{1+4a^2+4\sigma}). \tag{15}$$

Note that relation (14) is equivalent to that of Mullins and Sekerka [17] augmented by a new term added that is proportional to $\tilde{\alpha}$.

C. Discussion of the dispersion relation

The linear stability of the basic state with respect to the perturbations (13) is determined by the sign of $\sigma_r=\mathrm{Re}(\sigma)$. We focus on the neutral stability curves (NSCs), which are expressed in the form $M^{-1}=M^{-1}(a)$ defined implicitly by the dispersion relation and the condition of zero growth rate, i.e., $\sigma_r=0$. Unlike the Mullins-Sekerka case, $\omega=\mathrm{Im}(\sigma)$ is no longer zero, meaning that we expect critical modes to be traveling waves. Furthermore, for fixed a, up to three solutions $[M^{-1}(a),\omega(a)]$ are possible, depending upon the choices of the parameters. The consequences will be discussed below; mainly we focus on three dominant effects: (i) the nonconnectedness of the neutral stability curve, (ii) the contribution to the stabilization of the flat interface due to anisotropy, and (iii) the occurrence of a novel instability at relatively large values of k. All three cases are accessible to asymptotical analyses and these will be developed in subsequent sections.

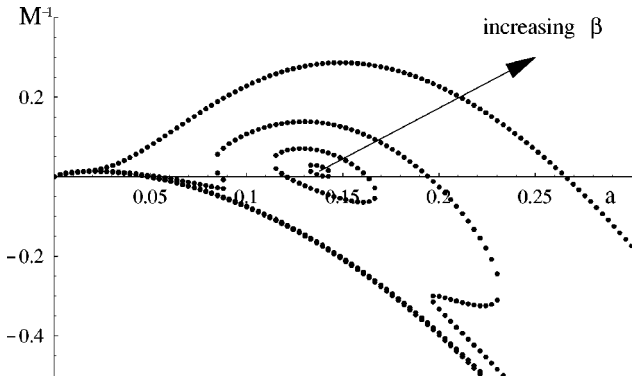

FIG. 1. Variation of the neutral stability curve under the effect of kinetic anisotropy. $k=0.18$, $\Gamma=10$, $p=0.1$, and $\beta=48\to100$. The full line is the NSC in the isotropic case, the dotted curve nearby is the one for small anisotropy ($\beta=100$) which appears to be a smooth deformation of the former. For smaller values of β (larger anisotropy) the NSC forms two folds which, at still smaller values, pinch off an isola, leaving a lower continuous branch passing through the origin. At some critical value of β, finally, the isola vanishes, leaving the continuous branch alone (which is not distinguishable from the one at the next higher value of β). Note that for uses of illustration only, parameters are chosen such that important parts of the curve are found at negative values of M^{-1} (and thus not of physical relevance).

The formation of multiple branches and isolas is most easily understood when looking at the changes the neutral stability curve undergoes with the variation of the parameters $\tilde{\alpha}$ and k. In Fig. 1, k is kept constant while $\tilde{\alpha}$ is varied (and we thus follow a vertical line in Fig. 2). In the isotropic case, i.e., $\tilde{\alpha}=0$, Mullins and Sekerka predict that all modes are linearly stable for large values of M^{-1} and a band of unstable modes exists for smaller values. For small enough $\tilde{\alpha}$, this picture is still valid, but the resulting neutral stability curve is now a smooth deformation of the one obtained pre-

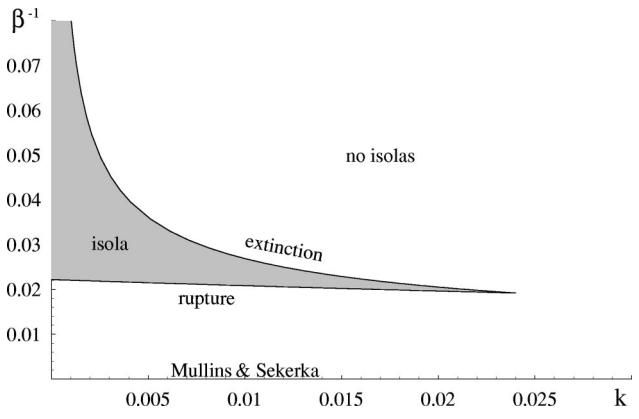

FIG. 2. Existence domain for isolas varying k and β ($\tilde{\alpha}=1/\beta p^2$). Isolas contract to a single point at the upper line, and they fuse to the lower (continuous) branch at the lower line. At the point of intersection of the two lines the neutral stability curve has a cusp. See Fig. 1 for the variation of the neutral stability curve in the vertical direction of the diagram and Fig. 3 for the variation in the horizontal direction. The parameters are $\Gamma=0.1$ and $p=0.1$. At least for small k, the upper line is well approximated by the Riley-Davis limit.

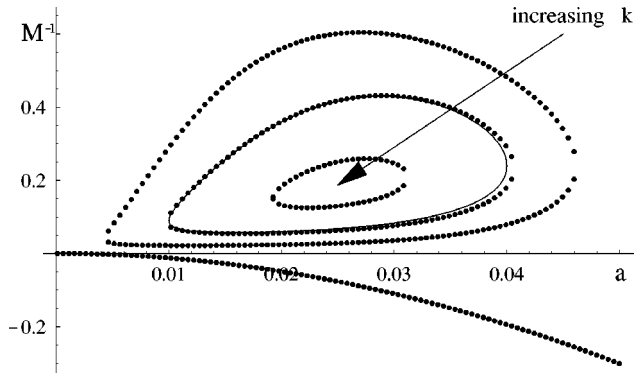

FIG. 3. Neutral stability curves for small k ($\Gamma=100$, $p=0.1$, $\beta=10$, and $k=2\times10^{-4}\rightarrow6\times10^{-4}$). The isolas, existing for some range of k, contract as the latter parameter increases. At some critical value the isolas contract to a single point and no longer exist for higher values. Beyond the point of extinction of the isola the plane front solution is dramatically stabilized. The stability is then dominated by the continuous part of the NSC which passes through the origin and which has a minimum at very small values of M^{-1} and a (see also Fig. 1). The solid curve shows the approximation of the neutral stability curve in the Riley-Davis limit. $1/\beta$ gives a measure of the anisotropy, $1/\beta=0$ corresponding to the isotropic case of Mullins and Sekerka.

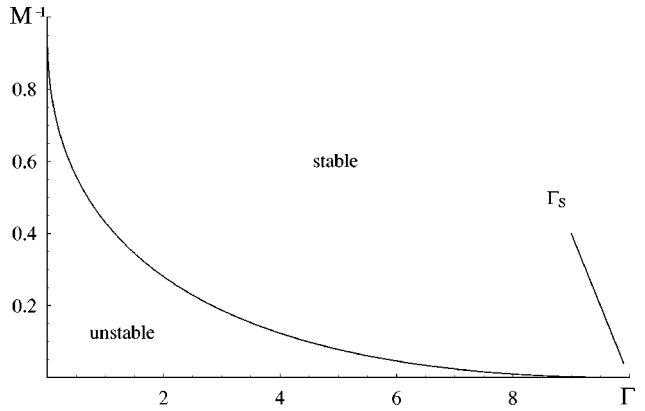

FIG. 4. Marginal stability diagram in the M^{-1}–Γ in the isotropic case ($k=0.1$). The plotted lines correspond to the local maxima of the neutral stability curve. The point of intersection with the Γ axis (at $\Gamma_s=10$) is the point of absolute stability.

viously, the modes being stabilized with respect to the isotropic case (at least for small enough k). Upon further increase of $\tilde{\alpha}$, three branches of the neutral stability curve become possible for certain wave numbers; more precisely, the formation of two folds is observed. Beyond a critical value of $\tilde{\alpha}$ the neutral stability curve is composed of a continuous part passing through the origin (but which is physically relevant only for small wave numbers) and of an isola which, in contrast to the isotropic case, contributes to instability only in finite intervals of wave-numbers and inverse morphological numbers M^{-1} (see also Fig. 3 for a case of very small k). Finally, for high enough values of $\tilde{\alpha}$, isolas no longer exist; neutral stability is then given by a curve similar to the Mullins-Sekerka one, but generally on different scales of wave numbers and morphological numbers. Similar things are found when $\tilde{\alpha}$ is kept constant and k is varied; Fig. 3 corresponds to following a horizontal line in Fig. 2. Increasing k, again there is a transition from the continuous, connected neutral stability curve to isolas, and further on the disappearance of the isolas and dominance of instability by the remaining continuous part of the curve. These transitions are summed up in the diagram of Fig. 2: Two lines define the existence domain of isolas. For low $\tilde{\alpha}$ there is a line of ''rupture'' where the isolas disconnect from the continuous neutral stability curve, and for large $\tilde{\alpha}$ and small k we find a line of ''extinction'' where the isolas retract to a single point and then vanish. At the point of intersection of the two lines, the neutral stability curve has a cusp.

It is worthwhile noting that in some cases linear theory predicts a ''stability window'' meaning that the domain of M^{-1} for which linear stability holds for all wave numbers is not necessarily the semi-infinite interval as was in the isotropic case, but can now be composed of a semi-infinite interval *and* a finite interval (the ''window''). This can be easily understood, when following vertical lines in Fig. 3. Note, however, that the physically relevant part of the continuous branch of the neutral stability curve is not clearly visible in the latter figure (this will become clearer below, when we discuss the absolute stability limit).

Summing up the observations made above, we can say that (i) one to three branches of the neutral stability curve are possible, (ii) they are not necessarily connected, and (iii) one of the branches always passes through the origin. We omit discussion of the cases where the isolas only exist for nonphysical (negative) values of M^{-1}.

Necessary conditions for the observation of isola are small k and large Γ. As long as $\tilde{\alpha}$ is taken to be small, it is the term $-\Gamma a^2$ that dominates the NSC for large a. If we take k to be even smaller (and dispense with the condition of large Γ) the stabilization at large wave numbers can be dominated by anisotropy. Or, expressed in physical terms, anisotropy plays a role analogous to that of surface energy, and its influence is strongly stabilizing. Γ can then even be chosen to be very small if the anisotropy is strong enough. However, it is not possible to replace the effect of capillarity completely by anisotropy; if $\Gamma=0$, large enough wave numbers are not stabilized.

In both of the above descriptions we have seen, for small values of k, that the effect of anisotropy is stabilizing; different results are found at larger values. In the isotropic case, i.e., in the analysis of Mullins and Sekerka [17], all modes are linearly stable for $\Gamma>k^{-1}$ since there the neutral stability curve only exists for negative (nonphysical) values of M^{-1} (see Fig. 4). This is the *absolute stability limit*, which is the complete stabilization of the flat interface by the effect of surface energy. When this limit is approached, the critical value for M^{-1}, as well as the critical wave number at which instability first occurs, tend to zero. Figure 5 shows this approach in the presence of kinetic anisotropy. The neutral stability curve now has two maxima: one, here occurring at high wave numbers, which is strongly influenced by Γ and which is directly related to the isotropic case, and another, occurring at low wave numbers which is hardly affected by Γ (see also Fig. 6). It is then easily seen that the latter becomes dominant at some value of Γ near the absolute stability limit. This is shown in Fig. 7. The new instability persists even far beyond the absolute stability limit of the isotropic

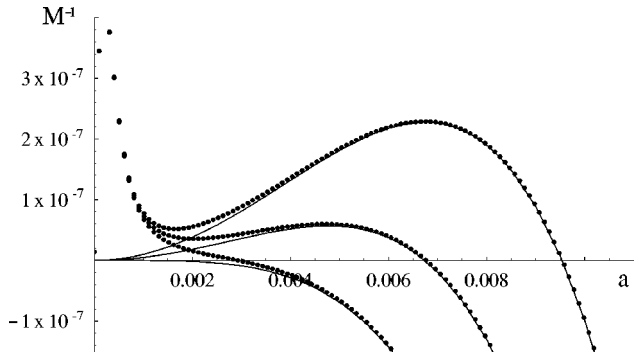

FIG. 5. Neutral stability curves near absolute stability of the isotropic case ($\Gamma = k^{-1}$). Parameters: $k = 0.1$, $\Gamma = 9.99$, 9.995, and 10.0, $p = 0.01$, and $\beta = 10^9$. Solid lines are NSC in the isotropic case, dots in the anisotropic case. In the isotropic case, the maximum of the NSC goes to zero and is taken at smaller and smaller wave numbers as the absolute stability curve is approached; when $\Gamma = k^{-1}$, it has a horizontal tangent at the origin. In the anisotropic case there is an additional maximum which becomes dominant for the instability for relatively large values of Γ. Figure 6 shows more details of the curve.

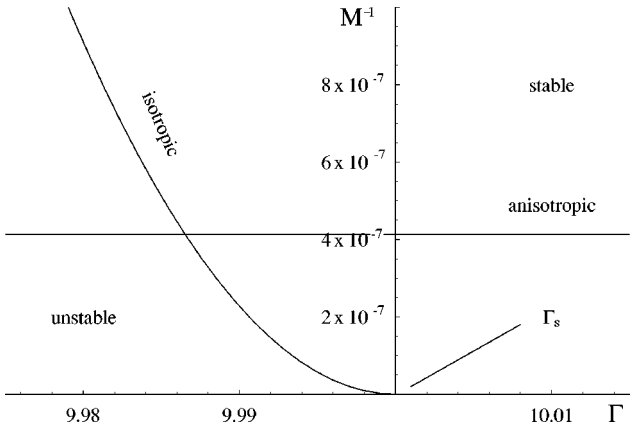

FIG. 7. Marginal stability diagram in the M^{-1}–Γ plane for Γ near $\Gamma_s \equiv k^{-1}$ ($k = 0.1$, $p = 0.01$, $\beta = 10^9$). Again, the plotted lines correspond to the local maxima of the neutral stability curve. The curved line is related to the isotropic case (see Fig. 4), the horizontal line to the new instability. At the point of intersection of the two curves, two modes with different length scales are marginally stable.

case as shown by Fig. 8. This figure also indicates that, in the presence of kinetic anisotropy, the absolute stability limit no longer exists (at least not in terms of the coordinates M and Γ).

For fixed temperature gradient G, the parameters M, Γ, and β depend on the dimensional parameters C_∞ and V, which are more useful for comparison to experiments. Figures 9 and 10 show the domains of stability in terms of the latter parameters, limited by the *marginal stability curves* which are determined by a condition of tangency for the neutral stability curves. Roughly speaking, the marginal stability curves are composed of two branches. The first one is found for low V and can be related to the isotropic case (anisotropy slightly stabilizes at very low V) and it is also related to the isolas, if they exist. The high velocity branch lies mainly above the upper part of the marginal stability curve of the isotropic case, and is thus beyond the absolute stability limit. It is uniquely due to the presence of kinetic anisotropy. Considering lines of constant C_∞ in Fig. 9, this gives the following picture: for C_∞ small enough, the planar front is linearly stable for any velocity. For large enough C_∞ it is unstable for some finite interval of velocities, i.e., stable for very low and for very high velocities. In an intermediate range, there are two intervals of velocities for which the planar front is unstable: one for low velocities, reflecting the classical Mullins-Sekerka instability, and one for high velocities owing its presence entirely to the kinetic anisotropy. The theory predicts a point, the point of intersection of the marginal stability curves, where the two phenomena are competing.

In concluding this section, we emphasize the following observations. As expected, a small kinetic anisotropy only yields moderate changes of linear stability, the most important effect being that the instability modes are traveling waves of a preferred direction rather than stationary cellular patterns. The changes can be dramatic if anisotropy is larger; branches of the neutral stability curve can disappear, resulting in a sudden stabilization of the flat interface. Different mechanisms of stabilization and destabilization can arise and eventually become more important than those related to the isotropic case.

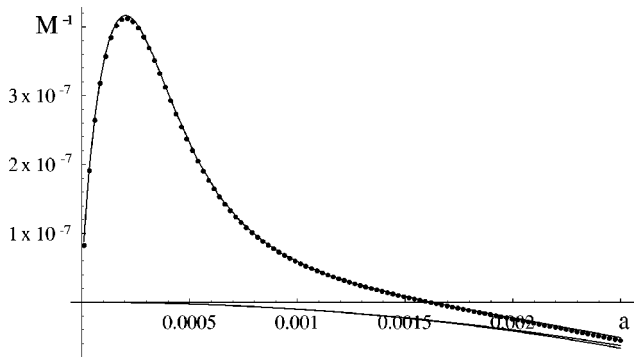

FIG. 6. Neutral stability curves computed from the full dispersion relation (dots), computed in the BASL (closely fitted solid line), and for the Brattkus-Davis limit in the isotropic case (downward parabola).

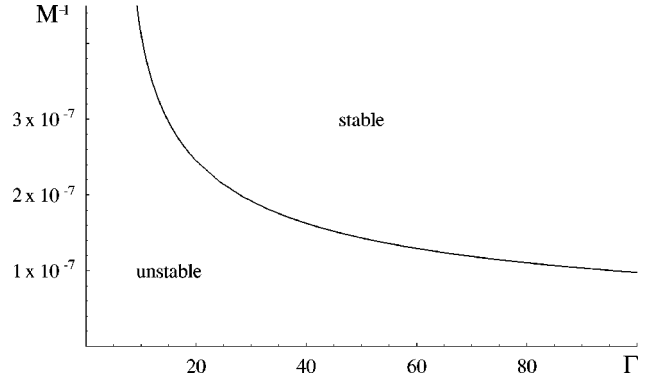

FIG. 8. Marginal stability curve in the presence of kinetic anisotropy. In contrast to the isotropic case, there no longer seems to be an absolute stability limit for the anisotropic model. The curve is the continuation of the one of Fig. 7 (note the different scales).

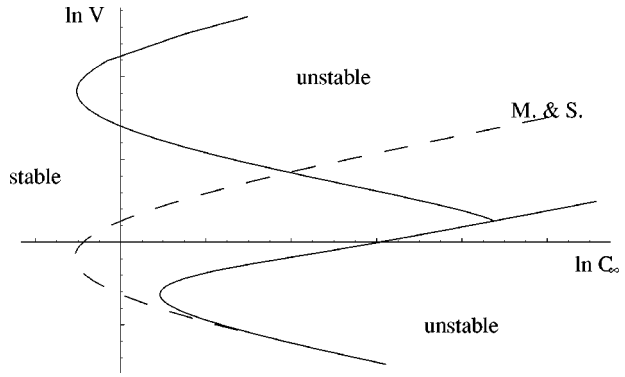

FIG. 9. Marginal stability curves for the parameters V and C_∞ (arbitrary units). The planar front is stable to the left of the curves and unstable to the right. The lower branch appears to be a smooth deformation of the curve computed in the isotropic case (dashed line). The upper branch is due to a new instability and is strongly related to the effect of kinetic anisotropy.

III. LONG-WAVELENGTH LIMITS

In this section we look more deeply into the effects of kinetic anisotropy by considering asymptotic expansions characterized by large wavelengths. Various long-wavelength limits have been considered in the isotropic case, an overview of which is presented in Ref. [12]; most of the limits considered here are closely related to them. After analyzing the dispersion relation, we shall derive nonlinear amplitude equations which govern the evolution beyond linear instability.

A. The Sivashinsky limit

Linear theory. Sivashinsky [11] takes the segregation parameter k to be very small, meaning that the solute rejection is almost complete. The NSC is then dominated by $1-\Gamma a^2$, except for a small boundary layer in the wave number a (see also Fig. 11). Therefore, we wish to define a length scale whose asymptotic limit well approximates the neutral stability curve at its maximum. Set $k=\varepsilon^2\kappa$, $\Gamma=O(1)$, and $M^{-1}=1-\mu\varepsilon$. There is some freedom for the choice of the scalings of the parameters p and β; here we take $p=O(\varepsilon^{1/2})$ and

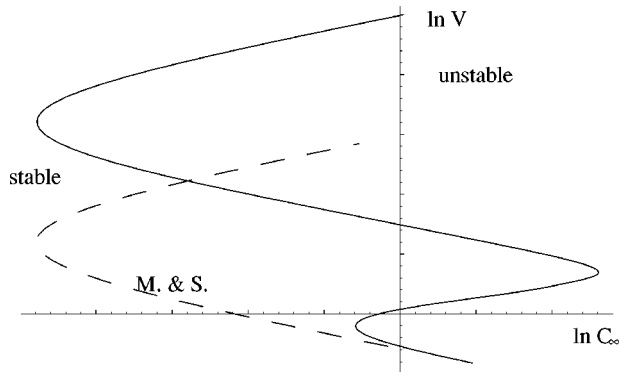

FIG. 10. Marginal stability curves for the parameters V and C_∞ (arbitrary units). The planar front is stable to the left of the curves and unstable to the right. The curve for the isotropic case is given for uses of comparison (dashed line). Again (as in Fig. 9), the classical instability is related to the lower part of the curve. For the parameters chosen for this plot the neutral stability curve has isolas.

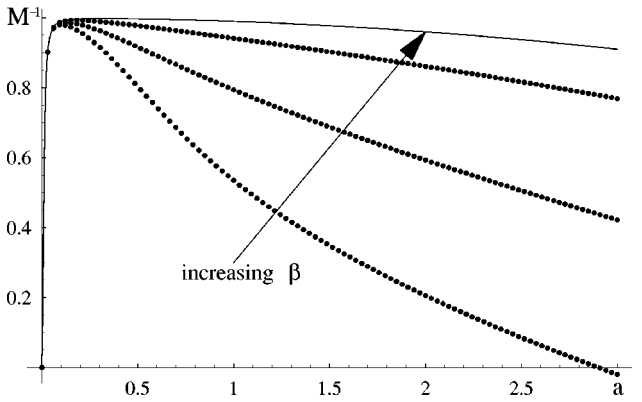

FIG. 11. Kinetic anisotropy stabilizes modes with high wave numbers in a way similar to surface energy. The effect is particularly pronounced when the segregation k is small. This makes an asymptotic limit similar to the one by Sivashinsky possible. Shown here are the neutral stability curves for various values of β (dots) and for the isotropic case (solid line). Parameters are $k=10^{-4}$, $\Gamma=0.01$, $p=0.1$, and $\beta=300,\ 150,\ 100$.

$\beta=O(\varepsilon^{-3/2})$. Consistent scalings for a and σ are then $a=O(\varepsilon^{1/2})$ and $\sigma=O(\varepsilon^2)$. The dispersion relation up to leading order then becomes

$$\mu-\frac{\kappa+\sigma}{a^2}-\Gamma a^2+i\tilde{\alpha}a=0 \tag{16}$$

and we see that the linear stability of the problem is not affected by the anisotropy at this order. The neutral stability curve turns out to be

$$\mu(a)=\frac{\kappa}{a^2}+\Gamma a^2 \tag{17}$$

on which the Hopf frequency $\sigma=i\omega$ varies as

$$\omega(a)=\tilde{\alpha}a^3. \tag{18}$$

Evolution equation. Let

$$C=\overline{C}+\sum_{j=1}^{\infty}\varepsilon^j C_j, \tag{19}$$

$$H=\varepsilon F \tag{20}$$

and solve Eqs. (8)–(10) at successive orders of ε. Then C_1 turns out to be

$$C_1=Fe^{-z} \tag{21}$$

and C_2

$$C_2=-(\mu F+\Gamma F_{xx}+\tilde{\alpha}F_x)e^{-z}. \tag{22}$$

At third order the diffusion equation is inhomogeneous and we have

$$C_3=\gamma e^{-z}-\delta_1 z e^{-z}, \tag{23}$$

where δ_1 is determined by the inhomogeneities

$$\delta_1=\mu F_{xx}+\Gamma F_{xxxx}-(FF_x)_x+\tilde{\alpha}F_{xxx} \tag{24}$$

and γ is determined by the kinetic law. The solute balance at this order imposes the solvability condition

$$-\delta_1=F_t+\kappa F \tag{25}$$

yielding the desired evolution equation

$$F_t+\kappa F+\mu F_{xx}+\Gamma F_{xxxx}+\tilde{\alpha}F_{xxx}-(FF_x)_x=0. \tag{26}$$

Equation (26) was obtained by Young *et al.* [10] in the framework of a simpler model for kinetic anisotropy, and a two-dimensional bifurcation analysis shows that nontrivial solutions bifurcate subcritically. The numerical simulation reveals, as expected, the formation of tilted cells. But although the shape of the cells seems to converge rapidly at the tips, the roots steepen until breakdown, a problem already known from the isotropic case (see Ref. [12]).

B. Evolution of anisotropy-stabilized modes (EVANST)

Linear theory. In this section we adopt essentially the same scalings as Sivashinsky [11] or Young *et al.* [10], but we now take anisotropy to be larger [i.e., $\tilde{\alpha}=O(1)$]. As we shall see, this asymptotic limit indicates that anisotropy is nearly sufficient to stabilize long-wavelength modes, though a very small contribution of capillarity is still requested to stabilize short-wavelength modes.

We now prefer to write the scaling as follows: $M^{-1}=1-\varepsilon^2\mu$, $k=\varepsilon^4\kappa$, $\Gamma=O(1)$, $\tilde{\alpha}=O(1)$, $a=O(\varepsilon)$, and $\sigma=O(\varepsilon^3)$. We look for the neutral stability curve and thus put $\sigma=i\omega$. When extracting equal powers of the dispersion relation, we first get at $O(\varepsilon)$

$$\omega(a)=\tilde{\alpha}a^3 \tag{27}$$

and then at the following order

$$\mu(a)=\frac{\omega^2(a)}{a^4}+\frac{\kappa}{a^2}+\Gamma a^2 \tag{28}$$

$$=\frac{\kappa}{a^2}+(\Gamma+\tilde{\alpha}^2)a^2. \tag{29}$$

Compared to the corresponding result of the preceding section, Eq. (17), we see that the term $\Gamma+\tilde{\alpha}^2$ plays the role of an effective surface energy in the long-wavelength approximation (see Fig. 11). However, when shorter waves are allowed, Γ cannot be set to zero.

Evolution equation. The derivation of the evolution equation requires the consideration of relatively high powers of ε. Introduce a slow time scale by letting $\partial_t\to\varepsilon^3\partial_t$, and expand the fields as follows:

$$C=\overline{C}+\sum_{k=1}^{\infty}\varepsilon^k C_k, \tag{30}$$

$$H=\sum_{k=1}^{\infty}\varepsilon^k F_k. \tag{31}$$

The first order yields

$$C_1=F_1e^{-z}. \tag{32}$$

The following order is then solved to give

$$C_2=(F_2-\tilde{\alpha}F_{1x})e^{-z}. \tag{33}$$

Next,

$$C_3=(F_3-\tilde{\alpha}F_{2x}-\mu F_1-\Gamma F_{1xx})e^{-z}. \tag{34}$$

At fourth order, where

$$C_4=\left[F_4-\tilde{\alpha}F_{3x}-\mu F_2-\Gamma F_{2xx}+p\tilde{\alpha}F_{1t}+\left(\frac{\tilde{\alpha}}{p}-\frac{p\tilde{\alpha}}{2}\right)F_{1x}^2\right]e^{-z}-\left(\tilde{\alpha}F_{1xxx}-\frac{1}{2}(F_1^2)_{xx}\right)ze^{-z} \tag{35}$$

there is a first condition arising from the solute balance

$$F_{1t}+\tilde{\alpha}F_{1xxx}-\frac{1}{2}(F_1{}^2)_{xx}=0. \tag{36}$$

Then, at fifth order

$$C_5=(\cdot)e^{-z}-[\mu F_{1xx}+\Gamma F_{1xxxx}-(F_1F_2)_{xx}+\tilde{\alpha}F_{2xxx}-F_1F_{1x}^2+F_1F_{1t}+3\tilde{\alpha}F_{1x}F_{1xx}-\tilde{\alpha}F_{1tx}]z\,e^{-z}. \tag{37}$$

We do not need the coefficient of e^{-z}, which could be determined by the kinetic law at this order. But the solute balance again imposes an equation, which has to be solved together with Eq. (36):

$$F_{2t}+\tilde{\alpha}F_{2xxx}-(F_2F_1)_{xx}=-F_{1T}-\kappa F_1-\mu F_{1xx}-\Gamma F_{1xxxx}+\tilde{\alpha}F_{1tx}-\tilde{\alpha}(F_{1x}^2)_x. \tag{38}$$

Below, we develop both a weakly nonlinear analysis, revealing the bifurcation structure near the onset of the linear instability, and a strongly nonlinear analysis, making predictions on the emerging interface shapes.

Bifurcation analysis. For the computation of the Landau equation of the critical modes, we combine Eqs. (36) and (38) by writing $u=F_1+\epsilon F_2$. Then, with a new small parameter δ, $\varepsilon=\delta^2$, we get the equation

$$u_t+\tilde{\alpha}u_{xxx}-\frac{1}{2}(u^2)_{xx}+\delta^2\{\kappa u+\Gamma u_{xxxx}+\mu u_{xx}-\tilde{\alpha}u_{tx}+\tilde{\alpha}(u_x^2)_x\}=O(\delta^4). \tag{39}$$

Introduce the multiple time scales $\partial_t=\partial_{t_0}+\delta^2\partial_{t_2}+\delta^4\partial_{t_4}+\cdots$, $\mu=\mu_C+\delta^2\mu_2+\cdots$, and expand $u=\delta v_1+\delta^2 v_2+\delta^3 v_3+\cdots$. From linear theory, the values of the critical wave number, the critical frequency and the critical control parameter are known,

$$a_C^2 = \sqrt{\frac{\kappa}{\Gamma + \tilde{\alpha}^2}}, \tag{40}$$

$$\omega_C = \tilde{\alpha} a_C^3, \tag{41}$$

$$\mu_C = 2\sqrt{\kappa}\sqrt{\Gamma + \tilde{\alpha}^2}. \tag{42}$$

The critical modes are traveling waves with phase speeds

$$c = \frac{\omega_C}{a_C} = \tilde{\alpha}\sqrt{\frac{\kappa}{\Gamma + \tilde{\alpha}^2}}. \tag{43}$$

We expand Eq. (39) and solve order-by-order in ε. The first-order equation is the linear problem with the solution

$$v_1 = A e^{i a_C x + i \omega_C t_0} + \text{c.c.} \tag{44}$$

At second order, the problem may be solved explicitly, the amplitudes turning out to be products in A and $\bar{A}$. At third order there is a solvability condition

$$A_{t_2} = \frac{i}{3\tilde{\alpha}} \sqrt[4]{\frac{\kappa}{\Gamma + \tilde{\alpha}^2}} A|A|^2. \tag{45}$$

The coefficient of the cubic term is imaginary, so that this equation does not give any information concerning the modulus of A, but it gives an amplitude-dependent correction to ω_C (or to the velocity c). The fourth-order equation may again be solved explicitly, and finally at fifth order there is another solvability condition which is the Landau equation that we have been seeking. After rescaling of the time t_4 it can be written as

$$A_{t_4} = (\mu_2 + i\mu_i)A - \frac{1}{2}\left(3 - \frac{\Gamma}{\tilde{\alpha}^2}\right)A|A|^2 + ibA|A|^4, \tag{46}$$

where b and μ_i are real constants, again contributing to a correction of ω_C. Note that μ_i appears as the only consequence of the high-order terms summarized as $O(\delta^4)$ in Eq. (39). The coefficient of the cubic term is real and can change its sign. If $\tilde{\alpha}$ is large enough with respect to Γ, then the bifurcation is supercritical, meaning that small traveling-wave solutions are expected to be observed beyond the threshold of linear instability. If $\tilde{\alpha}$ is small we recover the subcritical bifurcation of Sivashinsky (see previous section). Roughly speaking, we could say that in this particular limit the effect of anisotropy is to promote a smooth transition from the flat interface to a corrugated one.

Strongly nonlinear analysis. The bifurcation analysis of the previous section predicts the amplitude of sinusoidal front shapes close to the threshold of linear instability. It does not give any indications concerning the shape of the interface when nonlinear effects become more important. The strongly nonlinear analysis of this section has some similarities with the work of Merchant *et al.* [18] for a flat pulsating solidification front in the context of rapid solidification. It appears to be even closer to the recent investigations of Golovin and Davis [16] on a model of anisotropy for solidification into a hypercooled melt; its mathematical basis was elaborated by Bar and Nepomnyashchy [19]. It turns out, however, that the great number of parameters in our problem makes conclusive statements rather difficult, and we shall therefore not investigate the question of selection of amplitudes and velocities of the emerging patterns.

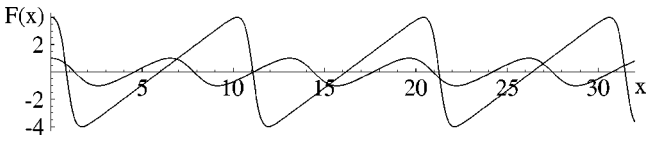

FIG. 12. Two solutions of Eq. (48). Small-amplitude solutions are sinusoidal whereas strongly preferred orientations develop for large amplitudes. The latter resemble facets.

Let us focus on Eq. (36). When looking for traveling-wave solutions of the form

$$F_1(t,x) = u(ct + x), \tag{47}$$

and after integrating once, u is found to be governed by

$$cu + \tilde{\alpha} u'' = uu', \tag{48}$$

or formulated as a first-order ODE:

$$q' = p, \tag{49}$$

$$p' = \tilde{\alpha}^{-1} q(p - c). \tag{50}$$

A first integral for this system is easily found in the form

$$K = \frac{1}{2\tilde{\alpha}} q^2 - p - c \ln|p - c|. \tag{51}$$

Solutions of Eq. (48) are then given as contours of constant K. For small amplitudes, they are nearly sinusoidal, suggesting a cell-shaped interface shape, as predicted by the bifurcation analysis. For larger amplitudes, these cells become more and more tilted and finally, as the amplitude gets very large, they are more and more facetlike (see Fig. 12). The front is then composed of nearly linear pieces ($p \approx c$) connected by sharp variations (where both q and p vary rapidly). This reflects the conflict of the interface trying to align with the crystal lattice while still remaining close to its equilibrium position.

C. The Brattkus-Davis limit

Linear theory. In the isotropic case, the critical wave number and the critical value of M^{-1} both tend to zero as $\Gamma \to k^{-1}$, and finally all modes are linearly stable when $\Gamma = k^{-1}$ (see Fig. 5). This limit, the absolute stability limit, already mentioned in the general discussion of the dispersion relation above, was used by Brattkus and Davis [13] for the derivation of a strongly nonlinear long-wavelength evolution equation by setting $\varepsilon = k^{-1} - \Gamma$, $M^{-1} = O(\varepsilon^2)$, $k = O(1)$, and $\Gamma = O(1)$. Wave number and growth rate are then to be taken as $a = O(\varepsilon^{1/2})$ and $\sigma = O(\varepsilon)$. If we now try to take into account the effect of anisotropy, two scalings seem to possible for p and β. Either we take $p = O(\varepsilon^{1/2})$ and $\beta = O(\varepsilon^{-5/2})$ or $p = O(1)$ and $\beta = O(\varepsilon^{-3/2})$, both yielding

$$M^{-1}=a^2-\frac{1}{k^2}[k(\sigma+a^2)+a^2](a^2+\sigma)+i\tilde{\alpha}a. \quad (52)$$

A problem arises when looking at the neutral stability curve in this limit. Set $\sigma=i\omega$ and separate the above equation into real and imaginary parts

$$M^{-1}=a^2-\frac{1+k}{k^2}a^4+\frac{\omega^2}{k} \quad (53)$$

and

$$\omega=\frac{\tilde{\alpha}k^2}{1+2k}a^{-1}. \quad (54)$$

We see that this scaling is inappropriate, as $\tilde{\omega}\propto a^{-1}$, and thus even for small $\tilde{\alpha}$ there is always a band of unstable long-wavelength modes. There is no simple way to circumvent this problem, but much is explained by the scaling developed in the next section.

D. Beyond the absolute stability limit (BASL)

Linear theory. The presence of anisotropy gives rise to a new long-wavelength limit unrelated to any limit of the isotropic case, stemming from the additional maximum of the neutral stability curve mentioned earlier in the discussion of the dispersion relation. Let us scale as follows: $M^{-1}=O(\varepsilon^2)$, $p=O(\varepsilon)$, $\beta=O(\varepsilon^{-4})$, $a=O(\varepsilon)$, and $\omega=O(\varepsilon)$. We determine the neutral stability curve by putting $\sigma=i\omega$. At order ε^2 we get

$$M^{-1}=(k^{-1}-\Gamma)a^2+\frac{\omega^2}{k}. \quad (55)$$

ω is determined at the following order by solving

$$\omega^3+a^2\omega-\frac{\tilde{\alpha}k^2}{1+2k}a=0. \quad (56)$$

The resulting curve $\omega=\omega(a)$ then grows as $a^{1/3}$ at the origin, and after having reached a maximum decays as a^{-1}. The neutral stability curve in terms of M^{-1} therefore has a vertical tangent at the origin, which is rather unusual. This is corrected by terms of the following order which introduce a singular perturbation near the origin. A more important observation is that we need to have $\Gamma\geqslant k^{-1}$ in order to make this limit work (although we may get an accurate description of the neutral stability curve near the origin when $\Gamma<k^{-1}$). In terms of the isotropic case we are here working beyond the absolute stability limit ($\Gamma=k^{-1}$). Figure 6 shows a comparison of the approximated and the full neutral stability curves. Note that the most important contribution to the neutral stability curve is now given by the frequency term $\omega(a)$. Numerical as well as asymptotic results seem to indicate that, in terms of Γ and M, there is no absolute stability limit anymore (see Fig. 8). In terms of V and C_∞, the instability is related to the upper (high velocity) branches of the marginal curves of Figs. 9 and 10.

Evolution equation. We allow amplitudes of unit order for H and expand the deviations from the basic state (12) in an asymptotic series:

$$H=\sum_{j=0}^{\infty}\varepsilon^j F_j, \quad (57)$$

$$C=\overline{C}+\sum_{j=1}^{\infty}\varepsilon^j C_j, \quad (58)$$

and introduce two time scales by setting $\partial_t\rightarrow\varepsilon\partial_t+\varepsilon^2\partial_T$. At first order, the diffusion equation together with the solute balance yields

$$C_1=F_{0t}e^{-z} \quad (59)$$

with which the equation for the interface dynamics is satisfied identically. At second order we may determine coefficients γ_k depending on F_0 such that

$$C_2=\sum_{k=0}^{2}\gamma_k z^k e^{-z} \quad (60)$$

satisfies the diffusion equation and the solute balance at this order

$$\gamma_0=-\frac{1}{k}(F_{0xx}+F_{0tt}), \quad (61)$$

$$\gamma_1=F_{0T}+F_{1t}-F_{0xx}-F_{0tt}-F_{0x}^2, \quad (62)$$

$$\gamma_2=-\frac{1}{2}(F_{0t}^2+F_{0tt}). \quad (63)$$

Interfacial kinetics now imposes the condition

$$(p+F_{0x})\{F_{0tt}+kM^{-1}F_0\}=0 \quad (64)$$

and for consistency we require the second expression to vanish, which is achieved by setting

$$F_0(t,T,x)=A(T,x)e^{i\omega_0 t}+\overline{A}(T,x)e^{-i\omega_0 t}, \quad (65)$$

$\omega_0=\sqrt{kM^{-1}}$. In a similar way as at the previous orders we solve the diffusion equation and the solute balance at third order by the ansatz

$$C_3=\sum_{k=0}^{3}\delta_k z^k e^{-z} \quad (66)$$

and after determination of the coefficients, the kinetic boundary condition becomes

$$F_{1tt}+kM^{-1}F_1+\mathcal{L}F_0+\mathcal{N}(F_0)-\tilde{\alpha}\frac{F_{1x}}{1+F_{1x}/p}=0, \quad (67)$$

where we have divided by $1+F_{1x}/p$. $\mathcal{L}$ and $\mathcal{N}$ are given by

$$\mathcal{L}F=2F_{Tt}+(1+2k)M^{-1}F_t-\frac{1+2k}{k}F_{txx}+kF_{xx}, \quad (68)$$

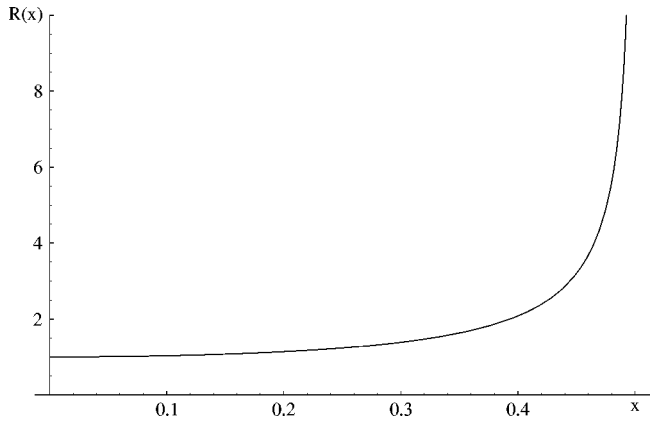

FIG. 13. Plot of the function $R(x)$ for $p=1$.

$$\mathcal{N}(F)=F_tF_{xx}+3kM^{-1}FF_t-2F_xF_{tx}. \tag{69}$$

For evident reasons there is a solvability condition of the form

$$2\omega_0A_T+\frac{1+2k}{k}\omega_0^3A-\frac{1+2k}{k}\omega_0A_{xx}+ik\tilde{\alpha}A_xR(|A_x|)=0, \tag{70}$$

where R is given by the integral

$$R(x)=\frac{1}{\pi}\int_0^{2\pi}\frac{\cos^2 t}{p+2x\cos t}dt. \tag{71}$$

Bifurcation analysis. A plot of the function R in Eq. (71) is shown in Fig. 13. A power series developed about $x=0$ shows that there is no linear term in x and the sign of the quadratic term is positive. This is sufficient to tell us that the underlying bifurcation problem for the critical modes gives only subcritical bifurcations.

Absent from this analysis are other nonlinearities, as appear in the Brattkus-Davis limit. They can be included by using different scalings of H and C. It turns out that the coefficients of the these nonlinear terms are such that they do not significantly influence the bifurcation behavior (i.e., the corresponding contribution to the Landau coefficient remains imaginary).

E. The Riley-Davis limit

Linear theory. A further case which we would like to take into consideration is the scaling used by Riley and Davis [12]: $\varepsilon=\Gamma^{-1/2}$, $M=O(1)$, $k=O(\varepsilon^2)$, $a=O(\varepsilon)$, and $\sigma=O(\varepsilon^2)$. We choose $p=O(\varepsilon)$ and $\beta=O(\varepsilon^{-1})$, leading to

$$M^{-1}=1-\frac{k+\sigma}{k+\sigma+a^2}-a^2+i\tilde{\alpha}a. \tag{72}$$

Splitting this equation into real and imaginary parts allows us to get the neutral stability curve

$$M^{-1}(a)=\frac{1}{2(k+a^2)}\{(1-2(k+a^2))a^2 \pm\sqrt{a^4-4\tilde{\alpha}^2a^2(k+a^2)^2}\} \tag{73}$$

on which the Hopf frequency ω is given by the following:

$$\omega(a)=\tilde{\alpha}a^3\{\tilde{\alpha}^2a^2+(M^{-1}+a^2)^2\}^{-1}. \tag{74}$$

Obviously the two branches do not exist for all values of a, suggesting that they approximate the isolas described above (see Fig. 3, for example). The curves only exist for values of k and $\tilde{\alpha}$ for which

$$k\tilde{\alpha}^2<\frac{1}{16}. \tag{75}$$

On the other hand, we recover the form of the neutral stability curve of the unperturbed case by simply putting $\tilde{\alpha}=0$, though this perturbation is singular.

Evolution equation. In this limit we are no longer allowed to work on the basis of the known solution $\overline{C}$ which immediately complicates the involved terms. Our ansatz for the solution is now

$$H=F, \tag{76}$$

$$C=C_0+\varepsilon^2C_1+\cdots \tag{77}$$

giving the following solution for C_0 at leading order:

$$C_0=1-Ae^{-z} \tag{78}$$

with A being defined as

$$A=1-M^{-1}F+F_{xx}+\tilde{\alpha}\frac{F_x}{1+F_x/p}. \tag{79}$$

The diffusion equation at first order is inhomogeneous, and its solution may be written as

$$C_1=\gamma e^{-z}+\delta_2ze^{-z}. \tag{80}$$

γ could be determined by the equation for the interface kinetics, but we shall not need it here. δ_2 is found determined by the diffusion equations to be

$$\delta_2=A_t+F_tA-A_{xx}-2F_xA_x-F_{xx}A-F_x^2A. \tag{81}$$

It is the solute balance which imposes the solvability condition, which turns out to be

$$A_t-A_{xx}-F_xA_x-F_{xx}A-k(1-A)=0 \tag{82}$$

or, in its expanded form,

$$F_t-MF_{txx}+MF_{xxxx}+(M-1-kM)F_{xx}+kF-\frac{1}{2}(F^2)_{xx} +\frac{M}{2}(F_x^2)_{xx}=\tilde{\alpha}M[B_t-B_{xx}+kB-(F_xB)_x] \tag{83}$$

with

$$B=\frac{F_x}{1+F_x/p}. \tag{84}$$

Bifurcation analysis. Near the onset of instability, we derive a Landau equation for the amplitude A of the single

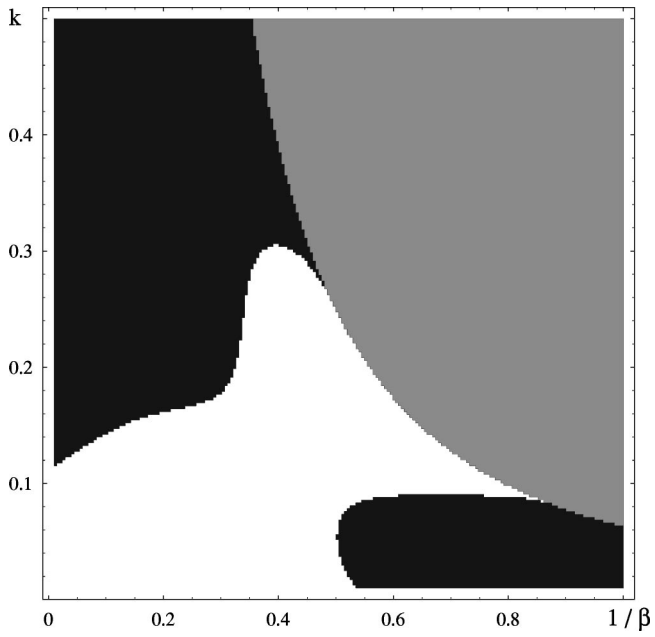

FIG. 14. Bifurcation structure in the Riley-Davis limit for the parameters k and $1/\beta$, with $p=0.1$. The bifurcation is supercritical in the black zone and subcritical in the white zone. There is no neutral stability curve for this limit in the gray zone, and our analysis does not apply. Note that we recover the transition from subcritical to supercritical bifurcations of the isotropic case $(1/\beta=0)$ which takes place at $k=1/9$.

mode $e^{ia_C x}e^{i\omega_C t}$. The evolution of the amplitude, which is supposed to vary on a slow time-scale τ, is governed by the Landau equation

$$A_\tau=\lambda A+bA|A|^2. \tag{85}$$

λ measures the departure from equilibrium, whereas b has to be computed; the general formulas are displayed in the Appendix. Depending upon the sign of b there are subcritical $(b>0)$ or supercritical $(b<0)$ bifurcations. Results of the computations are displayed in Fig. 14. First, note that (as mentioned above) the neutral stability curve does not exist for $k\tilde{\alpha}^2>\frac{1}{16}$. On the other hand the figure shows that, as expected, the results of the isotropic case are recovered when $\tilde{\alpha}\to 0$, i.e., that the bifurcation is supercritical for $k>\frac{1}{9}$ and subcritical otherwise. The most important change of the bifurcation structure is that supercritical bifurcations now occur also for small k, if $\tilde{\alpha}$ is large enough.

IV. CONCLUSION

Our investigations are based on a version of a classical one-sided model of directional solidification of a dilute alloy [17] including effects of kinetic anisotropy. In contrast to the physics of the underlying model, which is dominated by diffusion, mass conservation and surface energy, the mathematical formulation of the kinetic law relies upon considerations of the microscopic process of atoms or molecules attaching to step sites of a vicinal surface. Linear theory reveals three principal features associated with the new effects which connects the parts of this paper: (i) The possibility of *multiple branches* of the neutral stability curve, leading to the formation of isolas in some ranges of the parameter space, (ii) the important *stabilization* of the plane front in the case of *small segregation coefficients k*, and (iii) *destabilization* by the presence of a novel mode, typically related to *high velocities V* and *low wave numbers*.

In the wake of former asymptotic analyses of the isotropic model (Refs. [11–13]) we find asymptotic expansions of the dispersion relation which give some insight to the three observations stated above. Working with the scalings established for the linear theory, we then derived equations for the evolution beyond the threshold of instability.

As far as linear stability is concerned, only in the case of the Riley-Davis limit (see Ref. [12]) does the straightforward inclusion of the anisotropy terms within the asymptotic analysis of the isotropic case lead to interesting results; it gives a good description of the isolas and their extinction. The nonlinear evolution equation we find in this case turns out to be very complicated and we therefore restricted our attention to the investigation of the type of bifurcation. Both subcritical and supercritical bifurcations are found, and in contrast to the isotropic case, supercritical bifurcation is also possible for small values of k.

The Sivashinsky limit (see Ref. [11]) only predicts that the most unstable modes are traveling waves instead of stationary cells, but leaves the neutral stability curve unaffected. While this limit is modified in a way that emphasizes the fact that the critical modes are traveling waves, one sees that anisotropy strongly to stabilizes the planar front for small k. The eigenfunctions of the linear problem as well as comparison to the parent problem of directional solidification in presence of a shear flow [3] indicate that the physical explanation of this effect is a phase shift between interface deformations and the concentration profile. A first nonlinear evolution equation for this limit turned out to be the same as investigated by Young *et al.* [10] for a similar, but simpler model. The results they had obtained were that tilted cells bifurcate subcritically from the planar solution. In our modified version of this limit (i.e., when anisotropy is taken to be stronger), the subcritical bifurcation of Sivashinsky can become supercritical, i.e., that the interfacial pattern can appear in a smooth transition from the flat solidification front. Furthermore, a strongly nonlinear analysis predicts that the interface forms a periodic ''facetlike'' structure for larger amplitudes.

The Brattkus-Davis limit (see Ref. [13]) breaks down when the anisotropy terms are added naively, due to the presence of a novel instability which occurs on a different scale. The limit is applicable near the absolute stability limit of the isotropic case, i.e., near the complete stabilization of the planar interface by surface energy, but it cannot take into account the new instability which is almost unaffected by the presence of surface energy. We show how to establish a limit describing the new instability which is now purely due to the kinetic anisotropy (although capillarity can be included in the description). Thus, it seems that the tendency of the interface to align with the crystal direction by the effect of attachment kinetics is now stronger than any influence of the capillarity. It seems to be plausible that, at the high rates of solidification where the phenomenon occurs, the energy related to the attachment of the atoms dominates over surface energy. We do not give a detailed analysis of the evolution

equation that we derive in connection with this novel instability, and which could be called ''strongly anisotropic.'' However, a bifurcation analysis indicates that periodic solutions appear subcritically beyond the point of linear instability, and thus that we do not expect them to appear smoothly at the threshold of linear instability.

ACKNOWLEDGMENTS

The authors would like to thank Professor A.A. Golovin for his helpful suggestions. This research was partially supported by the Microgravity Research Division of NASA. H.P.G. acknowledges support from the Swiss National Science Foundation.

APPENDIX: THE LANDAU COEFFICIENT IN THE RILEY-DAVIS LIMIT

Defining

$$l_0 = -kM_C^{-1}, \tag{A1}$$

$$l_1 = (2i\omega_C + 4a_C^2 + k)(-4a_C^2 - M_C^{-1} + 2i\tilde{\alpha}a_C) + 4a_C^2, \tag{A2}$$

$$n_0 = -\frac{2k\tilde{\alpha}}{p}a_C^2, \tag{A3}$$

$$n_2 = -2a_C^2(M_C^{-1} + a_C^2) + \frac{\tilde{\alpha}}{p}a_C^2[k + 4a_C^2 + 2i(\omega_C + pa_C)], \tag{A4}$$

$$S_{\bar{A}B} = -a_C^2 M_C^{-1} + 2a_C^4 - \frac{4\tilde{\alpha}}{p}a_C^2[k + a_C^2 + i(\omega_C + pa_C)], \tag{A5}$$

$$S_{AC} = a_C^2 M_C^{-1}, \tag{A6}$$

$$S_{CC} = \frac{3i\tilde{\alpha}}{p^2}a_C^3[k + a_C^2 + i(\omega_C + pa_C)], \tag{A7}$$

$$R = a_C^2 + M_C^{-1} - i\tilde{\alpha}a_C, \tag{A8}$$

the Landau coefficient in Eq. (85) is given by

$$b = -\frac{1}{R}\left(S_{CC} - S_{\bar{A}B}\frac{n_2}{l_2} - S_{AC}\frac{n_0}{l_0}\right). \tag{A9}$$

[1] A. A. Chernov, *Modern Crystallography III: Crystal Growth* (Springer-Verlag, Berlin, 1984), pp. 116–122.
[2] A. A. Chernov, S. R. Coriell, and B. T. Murray, J. Cryst. Growth **132**, 405 (1993).
[3] S. R. Coriell, B. T. Murray, A. A. Chernov, and G. B. McFadden, Metall. Mater. Trans. A **27**, 687 (1996).
[4] S. R. Coriell and G. B. McFadden, in *Handbook of Crystal Growth*, edited by D. T. J. Hurle (Elsevier, Amsterdam, 1993), Vol. 1B, pp. 785–857.
[5] M. L. Frankel, Physica D **27**, 260 (1987).
[6] C. Misbah, H. Müller-Krumbhaar, and D. E. Temkin, J. Phys. I **1**, 585 (1991).
[7] A. Umantsev and S. H. Davis, Phys. Rev. A **45**, 7195 (1992).
[8] M. E. Glicksman and R. J. Schaefer, J. Cryst. Growth **1**, 297 (1967).
[9] S. R. Coriell and R. F. Sekerka, J. Cryst. Growth **34**, 157 (1976).
[10] G. W. Young, S. H. Davis, and K. Brattkus, J. Cryst. Growth **83**, 560 (1987).
[11] G. I. Sivashinsky, Physica D **8**, 243 (1983).
[12] D. S. Riley and S. H. Davis, SIAM (Soc. Ind. Appl. Math.) J. Appl. Math. **50**, 420 (1990).
[13] K. Brattkus and S. H. Davis, Phys. Rev. B **38**, 11 452 (1988).
[14] A. Novick-Cohen, Physica D **26**, 403 (1987).
[15] R. B. Hoyle, G. B. McFadden, and S. H. Davis, Philos. Trans. R. Soc. London, Ser. A **354**, 2915 (1996).
[16] A. A. Golovin and S. H. Davis, Physica D **116**, 363 (1998).
[17] W. W. Mullins and R. F. Sekerka, J. Appl. Phys. **35**, 444 (1964).
[18] G. J. Merchant, R. J. Braun, K. Brattkus, and S. H. Davis, SIAM (Soc. Ind. Appl. Math.) J. Appl. Math. **52**, 1279 (1992).
[19] D. E. Bar and A. A. Nepomnyashchy, Physica D **86**, 586 (1995).